Hybrid algorithms for spectral noise removal in hyper spectral images

Cite as: AIP Conference Proceedings **2271**, 030013 (2020); https://doi.org/10.1063/5.0025222
Published Online: 28 September 2020

Mohammed Abdulghani Taha, and Ganesh Babu Loganathan

Hybrid Algorithms for Spectral Noise Removal In Hyper Spectral Images

Mohammed Abdulghani Taha[1, a)] and Ganesh Babu Loganathan[2 b)]

[1,a)] *Lecturer, Computer Department,, Tishk International University, Erbil, KRG, Iraq*
[2,b)] *Assistant Professor, Research CenterTishk International University, Erbil, KRG, Iraq*

[a)]ganesh.babu@tiu.edu.iq, ganeshbabume8@gmail.com
[b)] mohammed.abdulghani@tiu.edu.iq

Abstract. The image acquired from a sensor is always degraded by some form of noise. The noise can be estimated and removed by the process of denoising. Recently, the use of Hybrid Algorithms for denoising has gained popularity. The most commonly used transformation are Discrete Cosine Transform (DCT) and Discrete Wavelet Transform (DWT). DCT has the property of more energy compaction and requires less resources for computational whereas DWT is a multi-resolution transformation. The proposed Hybrid Algorithms take advantage of both of the algorithms and this reduces the false contouring and blocking articrafts effectively. In this paper, the Hybrid Algorithms are evaluated for various images by differentiating with respect to Mean Square Error, Peak Signal to Noise Ratio, Coefficient of Variance, Structural Similarity Index and Mean Structural Similarity Index.

Keywords—CV, Denoising, MSE, PSNR, SSIM, MSSIM

INTRODUCTION

The noise free images are required for processing in satellite applications. MPEG-4[1]-[2] is the next generation visual coding standards which yield high versatility for evaluation of multimedia with visual objects based applications and upgrade the visual intensity at minimum rate of bits. Significantly used to access and manipulate individual objects. The arbitrarily shaped visual object must preserve its shape and texture. The existing methods include rectangle shape images and videos and coding like DCT coding and DWT coding. In conventional methods, the bounding box straighten the arbitrarily images, in the external side of the object pixel position values are padded and in the internal side, pixels of the object are coded and padded in the bounding box together, which might be inefficient [3]-[7]. The problem of removing the noise of visual objects without decomposing its attributes such as edges, textures, colors, contrast, etc., had been researched for the last two decades and many other types of denoising techniques have been developed. The total variance based noise removing method developed by Rudin et al.[25] had much influence in imagecommunity and inspire a large quantity of formulations for removing the noise of an image. In [8] - [10] the Non-Local Means (NLM) algorithm manages to correctly remove most of the noises, they tend tonot properly recover some of the image details. These methods also primarily deal with additive Gaussian noise, whereas for many images the noise model is unknown; in such cases, there is still ample room for improvement [10], [11],[12], [13].

This paper evaluates the Hybrid Algorithms as applied to denoise various satellite images. Section II deals about the Existing Transforms used for denoising the images. In Section III, Hybrid Algorithms designed for reducing articrafts are described. Section IV reports the result of the various algorithms and comparisons with other coding techniques for different images. Section V will conclude the paper.

International Conference on Mechanical, Electronics and Computer Engineering
AIP Conf. Proc. 2271, 030013-1–030013-13; https://doi.org/10.1063/5.0025222
Published by AIP Publishing. 978-0-7354-3999-3/$30.00

$$\boldsymbol{D_{DCT}(i,j) = \frac{1}{\sqrt{2N}} B(i)B(j) \sum_{x=0}^{N-1} \sum_{y=0}^{N-1} M(x,y)\, cos\left[\frac{2x+1}{2N} i\pi\right] cos\left[\frac{2x+1}{2N} j\pi\right] \quad ---} \qquad \boldsymbol{(1)}$$

EXISTING TRANSFORMS FOR DENOISING

A. Discrete Cosine Transform (DCT)

Input data points are indicated by DCT as a cosine function summation with various oscillating frequency and amplitude. The two main types of discrete cosine transform schemes are: discrete one dimensional cosine transform and discrete two dimensional cosine transform. Since an image is transformed as two 2-D matrix, two dimensional DCT is used. The 2D discrete cosine transform for a size x input sequence can be described as [14] [15]:

Where

$$B(u) = \begin{cases} \frac{1}{2} & if\ u = 0 \\ 1 & if\ u > 0 \end{cases}$$

x× y is the input data size M(x, y).

In DCT, each and every information were accommodating in a least number at low frequency coefficients which are easily affected by noise. The coefficients with least frequency are called as DC components and remaining coefficients are said to be AC components. Using 8×8 quantization table, the DCT coefficients are quantized as in the JPGE standard. The equation for two dimensional inverse DCT transform is given below.

$$D_{IDCT}(i,j) = \frac{1}{\sqrt{2N}} \sum_{x=0}^{N-1} \sum_{y=0}^{N-1} B(i)B(j)Ddequant(i,j) \cos\left[\frac{2x+1}{2N} i\pi\right] \cos\left[\frac{2x+1}{2N} j\pi\right] \quad -- \quad (2)$$

Where,

$$B(u) = \begin{cases} \frac{1}{2} & if\ u = 0 \\ 1 & if\ u > 0 \end{cases}$$

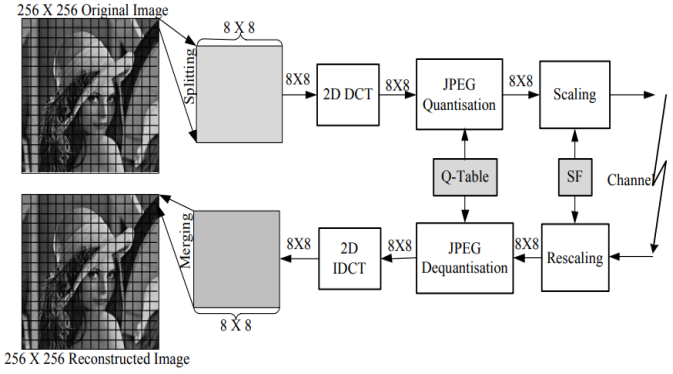

FIGURE 1 : Block Diagram of 2D-DCT

There exist certain limitations of DCT like blocking articrafts and False Contouring. The distortion like blocking articrafts occurs due to high compression rate and looks abnormally as large pixel blocks. The false contouring is due to smoothly graded area of visual objects which is distorted and appears as a contour map for some image[17]-[22]. The heavy quantization of the transform coefficients is the main reason for false contouring effect.

B. Discrete Wavelet Transform (DWT)

The DWT indicate the visual information as the sum of wavelet function, also called as wavelet with various location and numerous scale [8]. The high pass (detail) set and low pass (approximate) set of coefficients are the highlighted data. For transferring the input data, set of filters with low pass and high pass is utilized effectively. For this work filter kernel is $\begin{bmatrix} 1 & 1 \\ 1 & -1 \end{bmatrix}$. By factor 2 output of high and low pass filters are down sampled. This process is one dimensional DWT and the schematic is given in figure 2.

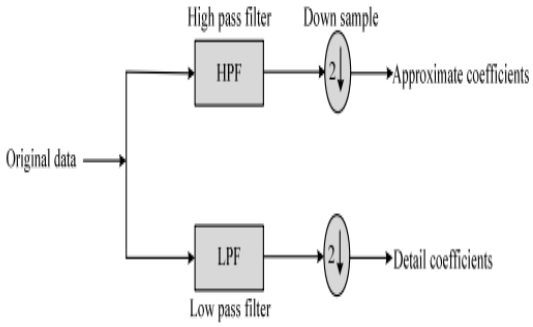

FIGURE 2 : Schematic of 1D forward DWT

In two dimensional DWT, low and high pass filter input data is moved in two distinct directions in row and column. In all the direction the outputs are down sampled by 2. The complete process is depicted in figure 3. The output is then obtained as 4 coefficients LL, HL, LH and HH. Row transformation makes the first alphabet and column transformation makes the second alphabet. The alphabet L represent signal with low pass and H indicates signal with high pass. In row, signal with low pass is represented by LH signal and in column, signal with high pass is represented by HH. LH signal consist of parallel elements, HL and HH consist of perpendicular and diagonal elements.

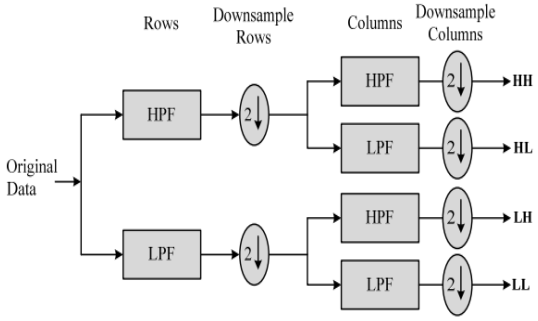

FIGURE 3 : Schematic representation of 2D forward DWT

As shown in Figure 4, during DWT reconstruction, input data can be obtained by disintegrating LL coefficient for levels with dissimilarity in multiple resolutions [38]. To redesign the output, reduced information is up sampled by factor 2. Then the signal was sent through the similar set of high pass and low pass filters in row and column. Complete recreating process was given in figure 5.

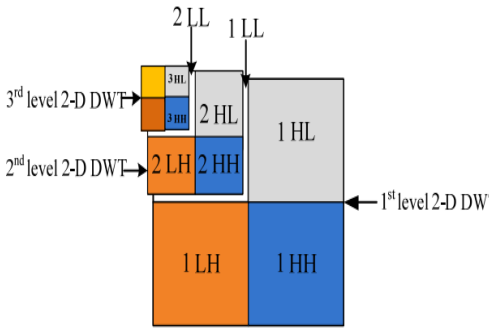

FIGURE 4 : Multilevel Forward DWT

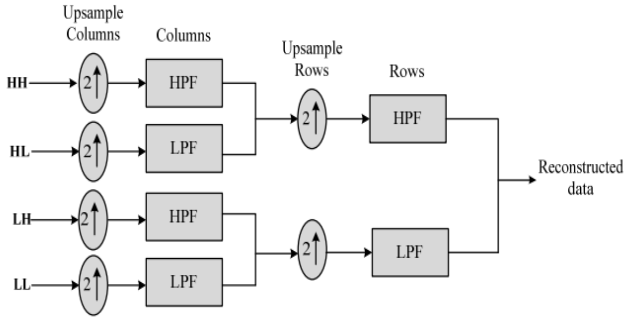

FIGURE 5 : Schematic representation of 2D Inverse DWT

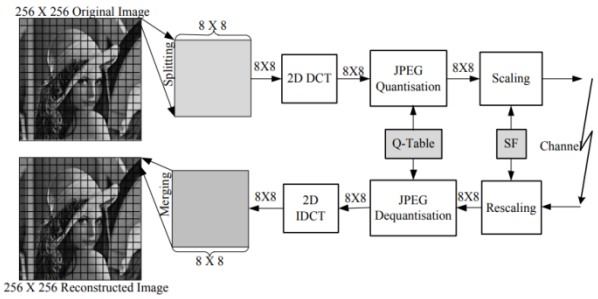

FIGURE 6 : Schematic representation of DWT Decomposition

The procedure persists for another level. The coefficients are split up by stable scaling factor to obtain required compression ratio. At last for reconstructing the information, the information was rescaled, padded with zeros and directed to the filters with wavelet. Figure 6 shows complete procedure of 2-D DWT compression and reconstruction.

PROPOSED HYBRID ALGORITHMS

The Discrete Cosine Transform and Discrete Wavelet Transform are used for denoising of images. DCT had more energy compaction property with less resources for computation, while DWT is multi resolution transformation. The proposed Hybrid Algorithms take advantage of both of the algorithms and thus reduce the false contouring and blocking articrafts effectively.

The algorithms are developed in such a way that the subsamples are processed in DCT while the main block is processed by DWT in Hybrid DWT-DCT as shown in figure 7.

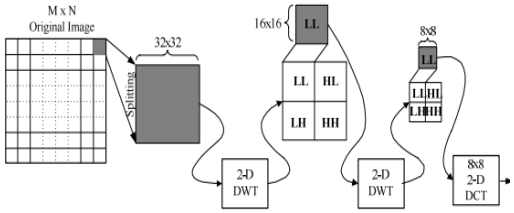

FIGURE 7 : representation of Hybrid DWT-DCT Algorithm

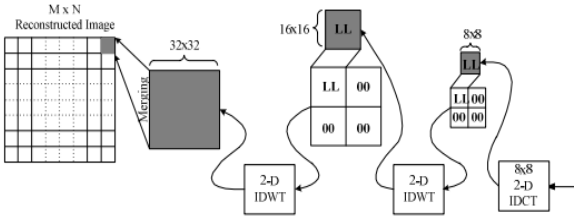

FIGURE 8 : Schematic representation of Inverse Hybrid DWT-DCT Algorithm

Algorithm for Hybrid DWT-DCT:

The sub sampling strategies based on DCT and DWT algorithms, discussed above, the Hybrid algorithms for a satellite image can be described as follows.

1) Read the input raw satellite vision data
2) Estimate the noise in the image.
3) Apply the 2-D DWT with proper sub sampling strategy.
4) choose the wavelet coefficients that are to be processed to perform 2-D DWT and obtain the second level low pass wavelet coefficients.
5) Perform the 2-D DCT with the obtained low pass coefficients.
6) Now perform 2-D Inverse DCT and subsequently two times 2-D Inverse DWT for reconstruction of denoised image.

Similarly, the subsamples are processed in DWT while the main block is processed by DCT in Hybrid DCT-DWT as shown in figure 9 and figure10.

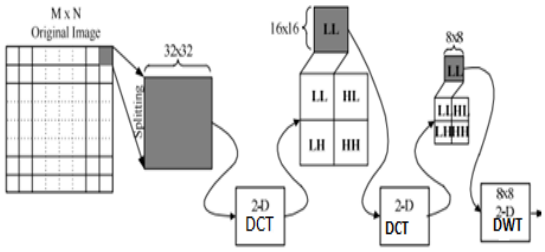

FIGURE 9 : Diagrammatic representation of Hybrid DWT-DCT Algorithm

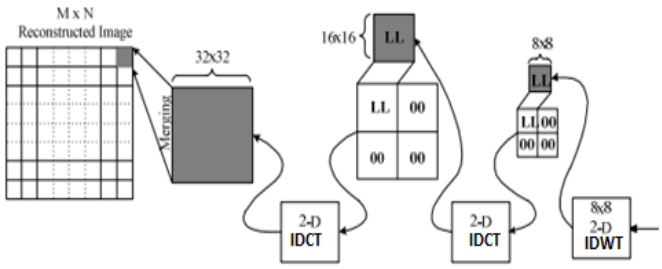

FIGURE 10 : Schematic diagram of Inverse Hybrid DWT-DCT Algorithm

RESULTS AND DISCUSSION

The Algorithms are coded and evaluated in MATLAB. The images considered for performance evaluation are shown in figures 11, 12, 13, 14 and 15. The Performance of hybrid algorithms is compared with existing algorithms based on MSE, PSNR, CV, SSIM and MSSIM parameters.

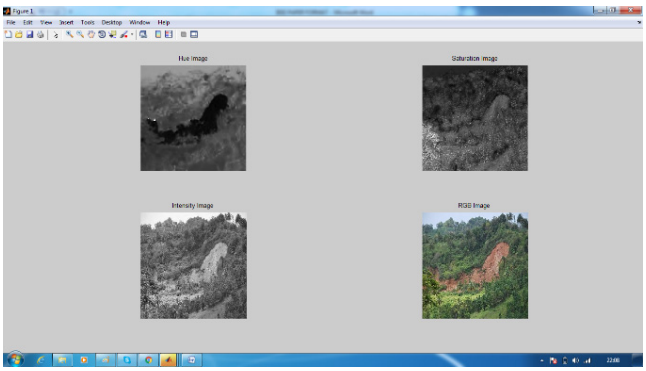

FIGURE 11 : Input Image – 1

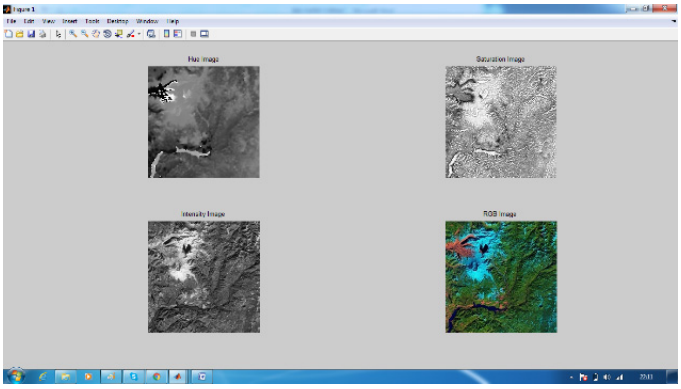

FIGURE 12 : Input Image - 2

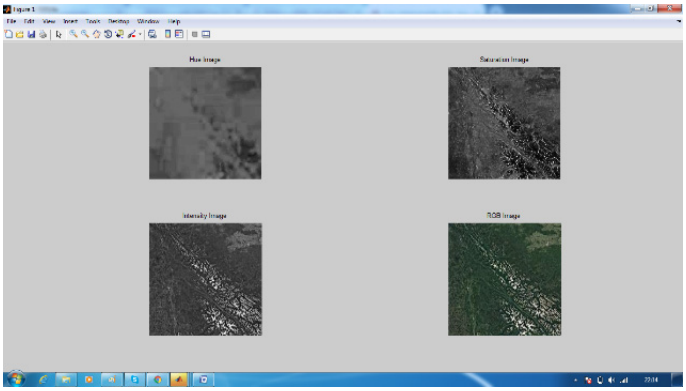

FIGURE 13 : Input Image - 3

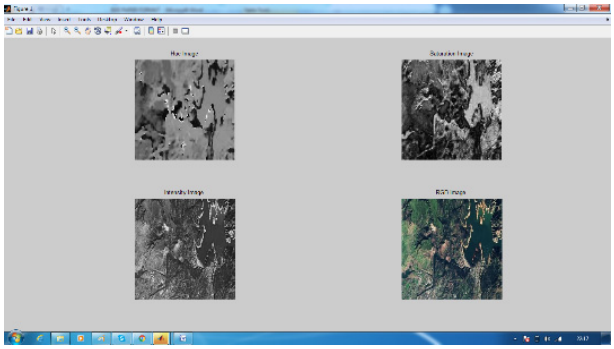

FIGURE 14 : Input Image - 4

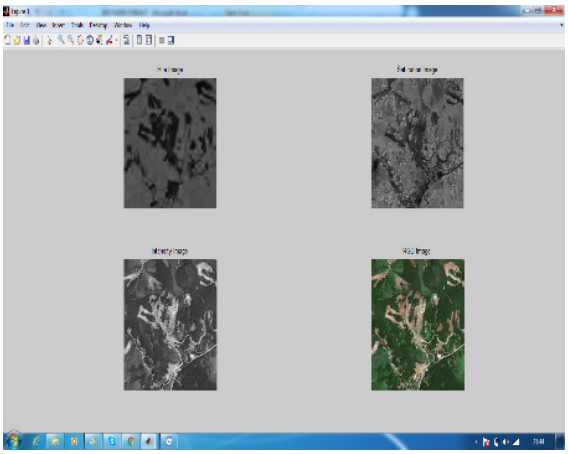

FIGURE 15 : Input Image - 5

The corresponding noise estimates are calculated for each channel as shown in figure 16, which shows that there exists noise in the images.

$$S(x,y) = f\big(l(x,y), c(x,y), s(x,y)\big) \qquad ------ \qquad (3)$$

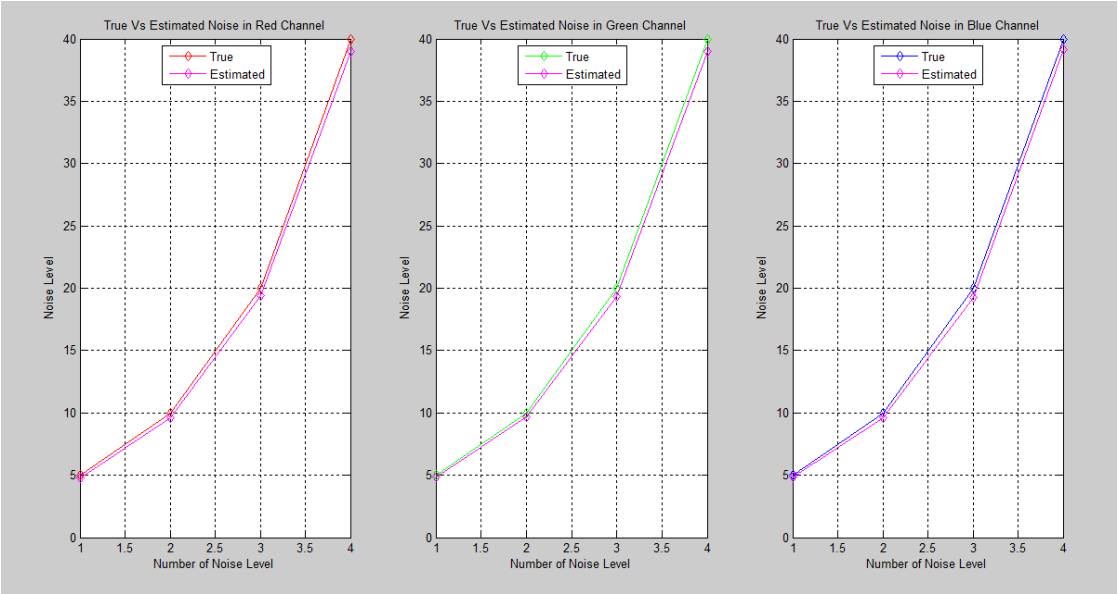

FIGURE 16 : Noise Estimate for Test Images

The ratio of the highest power signal to power with distorted noise which affects the standard is the peak signal to noise ratio.

$$PSNR = 20\log_{10}\left(\frac{MAX_f}{\sqrt{MSE}}\right) \quad -----(4)$$

$$MSE = \frac{1}{mn}\sum_{0}^{m-1}\sum_{0}^{n-1}\|f(i,j) - g(i,j)\|^2 \quad -------(5)$$

The PSNR must be as high as possible. The mean square error must be as low as possible.

$$MSSIM(X,Y) = \frac{1}{M}\sum_{j=1}^{M} SSIM(x_j, y_j) \quad -----(6)$$

The coefficient of variance is a measure of relative variability between the images, given by

$$\%CV = \frac{100\sqrt{\frac{\in X^2 - \frac{(\in X)^2}{N}}{N-1}}}{\bar{X}} \quad -----(7)$$

$\%CV$= percent coefficient of variation
$\in X$= sum of the assay values
N= number of assay values
$\in X^2$= sum of squares of all the values
$(\in X)^2$= square of the sum of all assay values
$\bar{X}$=arithmetic average of all assay values

The lower the value of the coefficient of variation the more the precise estimate

The method of estimating the similarity between two images was regarded as a Structural Similarity index. The SSIM index is also defined as a measure of quality of the visual object being compared by considering the quality of other visual data as perfect and is given by

$$SSIM(x,y) = [l(x,y)]^{\alpha}.[c(x,y)]^{\beta}.[s(x,y)]^{\gamma} \quad ------- \quad (8)$$

Comparison of structure s(x, y) was performed on the normalized signals $(x- \mu_x)/\sigma_x$ and $(y- \mu_y)/\sigma_y$.wherethe variables α, β and γ are used to vary the comparative significance of three elements.

The mean structural similarity for quantitative analysis of super-resolution image based on the size of the window which is given by

$$SSIM(x,y) = \frac{(2\mu_x\mu_y + C_1)(2\sigma_{xy} + C_2)}{(\mu_x^2 + \mu_y^2 + C_1)(\sigma_x^2 + \sigma_y^2 + C_2)} \quad -------- \quad (9)$$

The processed and reconstructed images for Hybrid DWT-DCT are shown in figure 17.

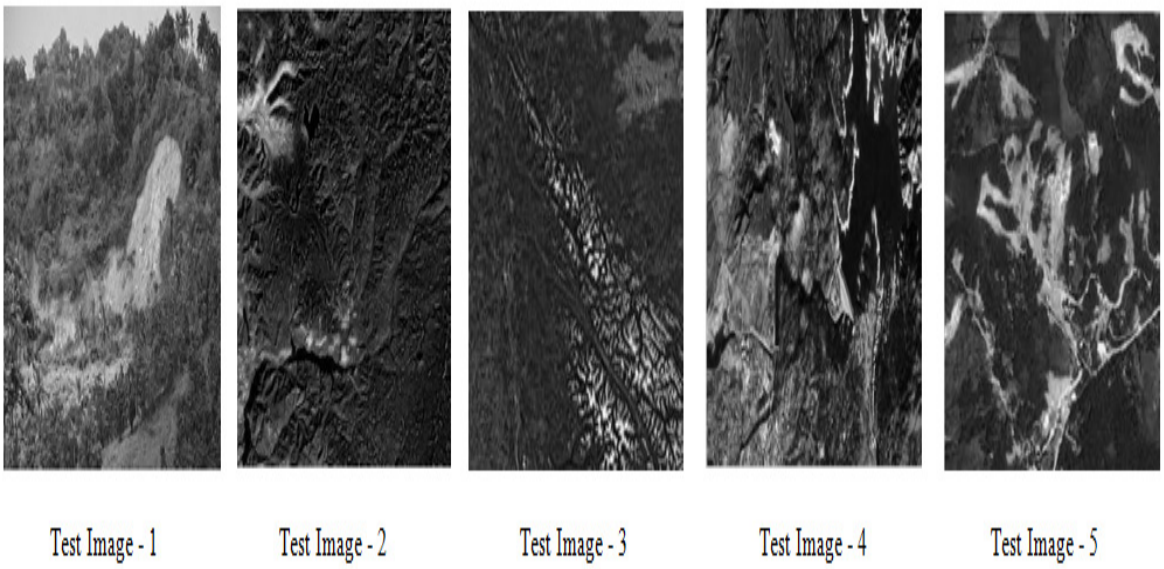

FIGURE 17 : Reconstructed Images of Hybrid DWT-DCT Algorithm

The Table 1 shows the various parameters used for comparing the denoising algorithms. From the table, it was clear that among all the algorithms Hybrid DWT-DCT algorithm has the best possible characteristics.

Table 1 Comparison of Denoising Algorithms based on various parameters

Method/ Images	Test Image – 1				
	MSE	PSNR	CV	SSIM	MSSIM
DCT	4.6175e+03	11.4867	45.8474	4.0682e-04	-5.1406e-04
DWT	751.0471	28.2299	47.0400	0.3054	0.1627
DWT-DCT	506.3219	29.8954	45.6364	0.9988	0.3229
DCT-DWT	5.1052e+03	25.8299	60.9139	0.4682	-0.0015
	Test Image – 2				
DCT	3.7023e+03	12.4461	76.9491	2.6988e-04	7.9426e-04
DWT	1.9393e+03	27.3432	76.5332	0.2397	0.1347
DWT-DCT	569.2167	29.6713	68.9416	0.9994	0.3385
DCT-DWT	2.9860e+03	26.7816	69.5503	0.2397	0.0988
	Test Image – 3				
DCT	2.8372e+03	13.6018	54.7035	0.0047	0.0062
DWT	788.5256	28.4754	49.1566	0.4241	0.2892
DWT-DCT	483.0586	31.9986	47.3910	0.9990	0.5239
DCT-DWT	798.7914	28.1722	51.0053	0.4241	0.2882
	Test Image – 4				
DCT	3.7059e+03	12.4418	69.7524	0.0074	0.0042
DWT	1.0954e+03	28.2315	57.8401	0.3804	0.2050
DWT-DCT	630.0937	30.6140	53.0960	0.9987	0.4252
DCT-DWT	1.2833e+03	27.0931	67.0268	0.3804	0.2025
	Test Image – 5				
DCT	250.7565	24.1383	62.9258	0.6489	0.9334
DWT	748.4971	28.4657	60.5928	0.4329	0.2543
DWT-DCT	383.4546	31.8982	54.2012	0.9986	0.4629
DCT-DWT	839.7779	28.7878	61.2381	0.4329	0.2489

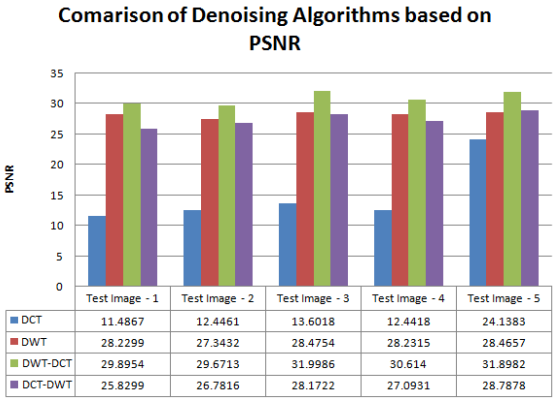

FIGURE 18 : Shows the maximum peak signal to noise ratio for Hybrid DWT-DCT Algorithm.

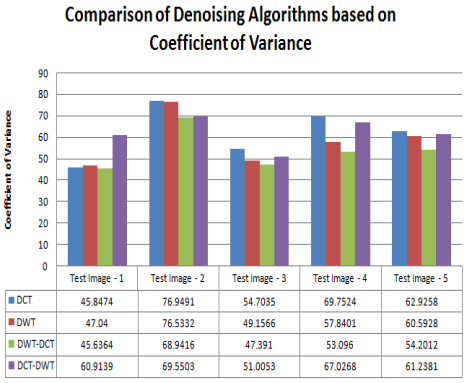

	Test Image - 1	Test Image - 2	Test Image - 3	Test Image - 4	Test Image - 5
DCT	45.8474	76.9491	54.7035	69.7524	62.9258
DWT	47.04	76.5332	49.1566	57.8401	60.5928
DWT-DCT	45.6364	68.9416	47.391	53.096	54.2012
DCT-DWT	60.9139	69.5503	51.0053	67.0268	61.2381

FIGURE 19 : shows that the coefficient of variance is minimum for Hybrid DWT-DCT Algorithm.

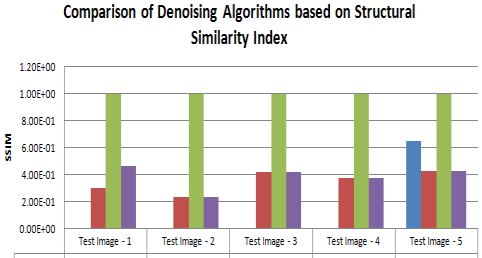

	Test Image - 1	Test Image - 2	Test Image - 3	Test Image - 4	Test Image - 5
DCT-DWT	0.4682	0.2397	0.4241	0.3804	0.4329
DWT-DCT	0.9988	0.9994	0.999	0.9987	0.9986
DWT	0.3054	0.2397	0.4241	0.3804	0.4329
DCT	4.07E-04	2.70E-04	0.0047	0.0074	0.6489

FIGURE 20 : shows that the Structural Similarity Index is maximum for Hybrid DWT-DCT Algorithm.

CONCLUSION

This paper presents description of Hybrid Algorithms for denoising the images captured by sensors. These algorithms use the DCT and DWT transforms for processing and take advantage of both transforms. These algorithms help in reducing false contouring and blocking articrafts effectively. Among these for a noisy satellite image, the Hybrid DWT-DCT algorithm proves to be a better choice as its PSNR has increased atleast by 13.5%, MSE and Coefficient of Variance is minimum and SSIM and MSSIM are improved when compared to DCT, DWT and Hybrid DCT-DWT Algorithms. Also the denoised images prove to have less noise in the images.

REFERENCES

1. R.Schafer and Heinrich-Hertz,"A Multimedia compression standard for interactive applications and services:MPEG4," Electronics and Communication Journal,vol.10, pp. 253-262, 1998.
2. A. Said and W. Pearlman, "Low-complexity waveform coding via alphabet and sample-set partitioning in visual communications and image processing," Proceedings of SPIE, pp. 25– 37, 1997.
3. S.-T. Hsiang and J. W. Woods, "Embedded image coding using zeroblocks of subband/wavelet coefficients and context modeling," Proceedings of ISCAS 2000 Geneva Circuits and Systems, vol. 3, pp. 662–665, 2000.

4. R.Costantini, J.Bracamonte, G.Ramponi, J.L.Nagel, M.Ansorge, and F.Pellandini, "Low complexity video coder based on discrete Walsh Hadamardtransform,"Proceedings of European signal processing conference, pp. 1217–1220, 2002.
5. M. Ezhilarasan and P. Thambidurai, "A hybrid transform technique for video coding," LNCS, vol. 4308, pp. 503–508, 2006.
6. U. S. Mohammed, "Highly scalable hybrid image coding scheme," Digital Signal Processing,Science Direct, vol. 18, pp. 364–374, 2008.
7. U. S. Mohammed and W. M. Abd-elhafiez, "Image coding scheme based on object extraction and hybrid transformation technique," International Journal of Engineering Science and Technology, vol. 2, no. 5, pp. 1375–1383, 2010.
8. T.-H. Yu and S. K. Mitra, "Wavelet based hybrid image coding scheme," Proceedings of IEEE International Circuits and Systems, vol. 1, pp. 377–380,1997.
9. R. Singh, V. Kumar, and H. K. Verma, "DWT-DCT hybrid scheme for medical image compression," Medical Engineering and Technology, vol. 31, pp. 109–122, 2007.
10. F. Zhijun, Z. Yuanhua, and Z. Daowen, "A scalable video coding algorithm based DCTDWT," IEEE International. Signal Processing and Information Technology, pp. 247–249,2003.
11. P. J. Paul and P. N. Girija, "A novel VLSI architecture for image compression," Proceedings of ISM'06 Multimedia Eighth IEEE International , pp. 794–795,2006.
12. K. A. Wahid, M. A. Islam, S. S. Shimu, M. H. Lee, and S. Ko, "Hybrid architecture and VLSI implementation of the Cosine-Fourier-Haar transforms," Circuits, Systems, and Signal Processing, vol. 29, no. 6, pp. 1193–1205, 2010.
13. S. Jiang and X. Hao, "Hybrid Fourier-Wavelet image denoising," Electronics Letters, vol. 43, no. 20, pp. 1081–1082, 2007.
14. A. H. Ali, "Combined DWT-DCT digital image water marking," Computer science, vol. 3, no. 9, pp. 740–746, 2007.
15. H. Qi, Q. Huang, and W. Gao, "A low-cost very large scale integration architecture for multistandard inverse transform," IEEE Transactions on Circuits and Systems II: Express Briefs, vol. 57, no. 7, pp. 551–555, 2010.
16. C. Fan and G. Su, "Fast algorithm and low-cost hardware-sharing design of multiple integer transforms for VC-1," IEEE Transactions on Circuits and Systems II: Express Briefs, vol. 56, no. 10, pp. 788–792, 2009.
17. C. P. Fan and G. A. Su, "Efficient fast 1-d 8 × 8 inverse integer transform for VC-1 application," IEEE Transactions on Circuits and Systems for Video Technology, vol. 19, no. 4, pp. 1–7, 2009.
18. K. Wahid, S.-B. Ko, and D. Teng, "Efficient hardware implementation of an image compressor for wireless capsule endoscopy applications," Proceedings of IEEE International Joint Conference Neural Networks, pp. 2761–2765,2008.
19. S. Shrestha and K. Wahid, "Hybrid DWT-DCT algorithm for biomedical image and video compression applications," Proceedings of IEEE International Conference on Information Sciences, Signal Processing and Applications, pp. 280–283,2010.
20. S. E. Ghrare, M. A. M. Ali, M. Ismail, and K. Jumari, "Diagnostic quality of compressed medical images: Objective and subjective evaluation," Proceedings of Second Asia International Conference Modeling & Simulation AICMS 08, pp. 923–927,2008.
21. D. S. Hands, Q. Huynh-Thu, A. W. Rix, A. G. Davis, and R. M. Voelcker, "Objective perceptual quality measurement of 3g video services," IEEE International Conference of 3G Mobile Communication Technologies 3G 2004, pp. 437–441, 2004.
22. H. S. Z. Wang, A. Bovik and E. Simoncelli, "Image quality assessment: From error measurement to structural similarity," IEEE Trans. Image Processing, vol. 13, no. 4, pp. 600–612, 2004.

23. Ganesh Babu Loganathan ; Praveen M. ; Jamuna Rani D. “Intelligent classification technique for breast cancer classification using digital image processing approach” Oct 2019 Available: https://ieeexplore.ieee.org/abstract/document/8882840
24. A.ShakinBanu , Dr.P.Vasuki , Ganesh BabuLoganathan , Dr. V.Srinivasa Raman , A.Yusuf Khan “Sparse Representation Based Despeckling of SAR Images using STDTCWT “ AUG 2019 Available: https://papers.ssrn.com/sol3/papers.cfm?abstract_id=3431020&download=yes
25. Suganthi K, IdrisHadiSalih, Ganesh BabuLoganathan and Sundararaman K, “A Single-switch Bi-polar Triple Output Converter with Fuzzy Control” , International Journal of Advanced Science and Technology Vol. 29, No. 5, (2020), pp. 2386 – 2400.